Communications in Mathematics and Applications
Vol. 15, No. 5, pp. 1579–1594, 2024
ISSN 0975-8607 (online); 0976-5905 (print)
Published by RGN Publications
DOI: 10.26713/cma.v15i5.2867

http://www.rgnpublications.com

Research Article

3-D Numerical Simulation of Pulsatile Blood Flow Through Healthy and Stenosed Aortoiliac Bifurcation

Josephina Harris*, Bhavna Singh Ghosh and Ajit Paul

Department of Mathematics and Statistics, Sam Higginbottom University of Agriculture, Technology and Sciences, Prayagraj 211007, Uttar Pradesh, India
***Corresponding author:** josephinaharris29@gmail.com

Received: August 27, 2024 **Accepted:** November 23, 2024

Abstract. The objective of this study is to examine the effect of pulsatile flow of blood on hemodynamic parameters in aortoiliac bifurcation with 0% and 71% occlusion in the infrarenal aorta. The three-dimensional model with 0% stenosis was generated from Magnetic Resonance Imaging data; further the 3D model with severe stenosis was constructed. Blood was considered Newtonian in nature and the two-equation k-ε turbulence model was used to simulate the flow. Maximum and minimum pressure drop was recorded at peak systole and diastolic phase, respectively across the severe stenosis. Maximum velocity is attained at peak systole, while the streamlines show a chaotic nature due to the presence of severe stenosis. The velocity profiles at the sites of interest were examined for both the models, at the throat of severe stenosis the velocity profile becomes asymmetric, owing its asymmetry to the formation of vortices and curvature of the artery. WSS variation was seen majorly at the throat of stenosis with maximum WSS at peak systole. Cardioid shaped region of high turbulent kinetic energy was identified in the post stenotic region in transverse section of model with severe stenosis. The results of this study suggest that the effects of pulsatile flow of blood on hemodynamic parameters is exacerbated due to severe stenosis in Aortoiliac Bifurcation. Using computational methods for investigating the changes in hemodynamic indices and flow patterns governed by pulsatile flow of blood will help in developing more specific and non-invasive medical interventions for *Aortoiliac Occlusive Disease* (AIOD).

Keywords. Computational fluid dynamics, Blood flow, Aortic bifurcation, Wall shear stress, Turbulent kinetic energy, OSI

Mathematics Subject Classification (2020). 76Z05, 76M12, 76-10, 92C10

Copyright © 2024 Josephina Harris, Bhavna Singh Ghosh and Ajit Paul. *This is an open access article distributed under the Creative Commons Attribution License, which permits unrestricted use, distribution, and reproduction in any medium, provided the original work is properly cited.*

1. Introduction

Global health reports exhibit increasing mortality and morbidity trends due to cardiovascular diseases accentuating the enormous burden of CVDs (Banerjee *et al*. [7], Faghy *et al*. [17], and Oliveira *et al*. [38]) on the healthcare system and economies. CVDs encompass a broad spectrum of disorders of the heart and blood vessels. Atherosclerosis is a complex, multifactorial inflammatory disease (Rocha *et al*. [35]) of the vascular system and is the most significant underlying pathology of CVDs including stroke, coronary artery disease, carotid artery disease and peripheral artery disease (Libby *et al*. [21]). The initiation and progression of atherosclerosis is dictated by the interactions between the hemodynamic and biomechanical forces [24]. Atherosclerosis development in the infrarenal abdominal aorta, iliac and femoropopliteal artery is referred as Aortoiliac occlusive disease (Paisley *et al*. [29]).

Asymptomatic atherosclerosis may remain undiagnosed and turn into a silent killer over time. Therefore, development of tools for early detection and prediction of vascular pathologies are necessary. By identifying the precursors and effects of arterial diseases, necessary medical interventions can be sought, thus, preventing any deadly consequences. Numerous approaches have been employed for the study of hemodynamics of stenosed and healthy arteries including Clinical Imaging Techniques (Engelhard *et al*. [15, 16]), in Vitro Flow models (Ahmed and Giddens [2, 3], Clark [14], and Young [40]) and Computational Fluid Dynamics (CFD). CFD simulations have emerged as a valuable tool owing to their advantages over traditional techniques. It is a cost-effective, non-invasive approach for which geometrical models can be constructed based on medical imaging data and simulations can be carried out for different conditions, thus providing crucial pieces of information. Several works have been carried out using numerical simulations for the study of hemodynamics in different geometries ranging from idealized geometries (Nadeem *et al*. [26]), carotid artery (Gay and Zhang [18], Karvelas *et al*. [19], Lopes *et al*. [22], and Moradicheghamahi *et al*. [25]), coronary artery (Abbasian *et al*. [1], Wendt [5], Carvalho *et al*. [12], Pandey *et al*. [30, 31], Rizzini *et al*. [34]), femoral artery (Amiri *et al*. [4], and Barber [8]), renal artery (Andayesh *et al*. [6]), aortic arch with diseased descending aorta (Bit *et al*. [9]).

Carneiro *et al*. [10] compared WSS, velocity profile and recirculation zones for Newtonian and non-Newtonian blood flow in the abdominal aorta bifurcation using an idealized geometrical model. Oliveira *et al*. [28] studied the Newtonian and non-Newtonian blood flow behavior in a patient-specific abdominal aortic bifurcation model. Carvalho *et al*. [11] conducted a numerical study of blood flow in simplified and realistic aorta-iliac bifurcation models using the k-ε model; the flow patterns and recirculation zones were analyzed alongwith distribution of velocity and WSS in the geometries.

CFD aids in unravelling the enigmatic interplay between atherosclerosis and hemodynamics; certainly, contributing to the understanding of this complex malady. This paper presents a numerical study of the effect of pulsatile blood flow on pressure, velocity, WSS and OSI distribution in 0% and severely stenosed aortoiliac bifurcation. Further, the turbulence in severely stenosed case is inspected using k-ε model.

Two models were employed in the study; model A represents the vasculature with 0% stenosis and is considered as the base model while model B represents the diseased condition

with 71% stenosis in the infrarenal region of the aorta. The hemodynamic parameters and flow patterns in both models are meticulously analysed for four-time frames. The impact of pulsatile blood flow on the turbulent kinetic energy in case of severe stenosis is further discussed.

2. Methodology

The algorithm of CFD modeling adopted for this study involves the selection and construction of both the models, meshing of the geometries and numerical solution of mathematical equations with suitable boundary conditions which define the hemodynamic behaviour. The results are post-processed for the variables of interest which are analysed and compared for both cases.

2.1 Geometry Construction and Meshing

The geometry of the aorta consists of side branches and bifurcates into the common iliac arteries. Its simplified or idealised model cannot imitate the real flow features, hence realistic models of the truncated aortoiliac bifurcation are constructed to include the effects of curvature. The 3D CAD model with 0% stenosis was generated from Magnetic resonance imaging data of 67yrs old healthy male obtained from Simtk.org in DICOM format (Wilson *et al*. [39]). Assuming axisymmetric development of stenosis a realistic model with 71% stenosis in the infrarenal region of the aorta was constructed. The constructed geometries were refined of all the interferences on their surface and imported into ANSYS Workbench 22.

(a) Model A **(b)** Model B

Figure 1. Volumetric mesh

The meshing of models was done on ANSYS 2022. The surface mesh for both the models was generated and five boundary layers were added at the boundary for refining the mesh near the walls, inlet and outlet faces. The volumetric mesh as shown in Figure 1 was generated with polyhedral elements with 86156 cells for Model A and 84367 cells for Model B. Polyhedral cells were used owing to their superiority in terms of better convergence and higher accuracy. The mesh independence test was carried out for Model A with the number of elements ranging from 28627 to 158146 as given in Table 1.

Table 1. Mesh independence study by varying number of elements

Mesh	Number of elements	Area-weighted average of wall-shear [Pa]
1	28627	1.7449
2	30363	1.7504
3	69112	1.7612
4	86156	1.7620
5	112997	1.7624
6	158146	1.7621

2.2 Mathematical Model

The descending aorta is the largest artery in the human anatomy, both in length and diameter, thus, the flow of blood can be assumed to be Newtonian (Paisley *et al*. [29]), unsteady, turbulent and incompressible. Blood density and viscosity were assumed to be 1060 kg/m^3 and 0.004 kg/(ms), respectively. The flow is governed by the three-dimensional equations of conservation of mass and momentum (2.1) and (2.2), respectively (Wendt [5]) and turbulence was modeled by the standard two-equation k-ε model given by eq. (2.3) and (2.4), along with enhanced wall treatment, providing a better approximation for the rigid wall,

$$\nabla\cdot\vec{v}=0, \tag{2.1}$$

$$\frac{\partial}{\partial t}(\rho\vec{v})+\rho(\vec{v}\cdot\nabla)\vec{v}=-\nabla p+\nabla\cdot(\bar{\bar{\tau}}), \tag{2.2}$$

$$\frac{\partial}{\partial t}(\rho k)+\nabla\cdot(\rho\vec{v}k)=\nabla\left[\left(\mu+\frac{\mu_t}{\sigma_k}\right)\frac{\partial k}{\partial x_j}\right]+G_k-\rho\varepsilon, \tag{2.3}$$

$$\frac{\partial}{\partial t}(\rho\varepsilon)+\nabla\cdot(\rho\vec{v}\varepsilon)=\nabla\left[\left(\mu+\frac{\mu_t}{\sigma_\varepsilon}\right)\frac{\partial\varepsilon}{\partial x_j}\right]+C_{1\varepsilon}\frac{\varepsilon}{k}G_{k}-C_{2\varepsilon}\frac{\varepsilon^2}{k}, \tag{2.4}$$

where $\vec{v}$ is the velocity vector, ρ fluid density, p pressure, τ the stress tensor, k turbulent kinetic energy, ε dissipation rate, μ the viscosity, G_k represents the generation of turbulent kinetic energy, σ_k and σ_ε are turbulent Prandtl numbers for k and ε, 1.0 and 1.3, respectively, $C_{1\varepsilon}=1.44$ and $C_{2\varepsilon}=1.92$ are constants. The turbulent viscosity μ_t is a combination of k and ε given by eq. (2.5) as

$$\mu_t=\rho C_\mu\frac{k^2}{\varepsilon}, \tag{2.5}$$

where $C_\mu=0.09$.

2.3 Boundary Conditions

At the aorta inlet a pulsatile velocity profile, mathematically as given by eq. (2.6), is applied by a user-defined function, and at the left and right iliac outlets constant pressure of 13332 Pa is applied (Sinnott *et al*. [36]). The wall is assumed to be stationary with no-slip condition,

$$v(t)=\begin{cases}0.5\sin[4\pi(t+0.0160236)], & \text{if } 0.5n<x\le 0.5n+0.218,\\ 0.1, & \text{if } 0.5n+0.21<x\le 0.5(n+1),\end{cases}\qquad n=0,1,2,3\ldots. \tag{2.6}$$

2.4 Numerical Solution

The numerical simulation was carried out using the finite volume method on ANSYS FLUENT. FVM is based on the conservation laws and ensures conservation of mass, momentum and energy at subdomain level. It is well-suited for problems of fluid flow, where mass, momentum and energy conservation for each variable is essential (Wendt [5]).

The conservation equations are discretised into algebraic equations, the coefficient matrix of which was solved by Gauss-Seidel point implicit linear equation solver. The "standard" scheme was used for solving the pressure equation, second order upwind scheme for discretizing the momentum and turbulence dissipation, while the first order upwind scheme was used for discretising the turbulent kinetic energy. The fluid flow equations were resolved by using the segregated solver with the *Semi-Implicit Method for Pressure Linked Equations* (SIMPLE) algorithm. The equations were solved sequentially and the solution was obtained iteratively, the process was continued until the desired convergence was achieved. The convergence criteria were set at continuity, velocity and turbulence residuals $< 10^{-5}$.

3. Results and Discussion

The truncated 3D anatomical geometries comprising the abdominal aorta bifurcating into the common iliac arteries manifest different flow features in different regions; hence, the examination of flow parameters in the regions of interest is crucial. A temporal study is carried out on the flow features recorded at four time instances T1, T2, T3 and T4, as shown in Figure 2. T1 lies in the acceleration phase where the velocity increases continuously, T2 is the time where velocity reaches its peak, T3 lies in the deceleration phase and T4 is the time where the minimum velocity is recorded. The study of blood flow and related parameters was carried out to capture the effect of pulsatile blood flow.

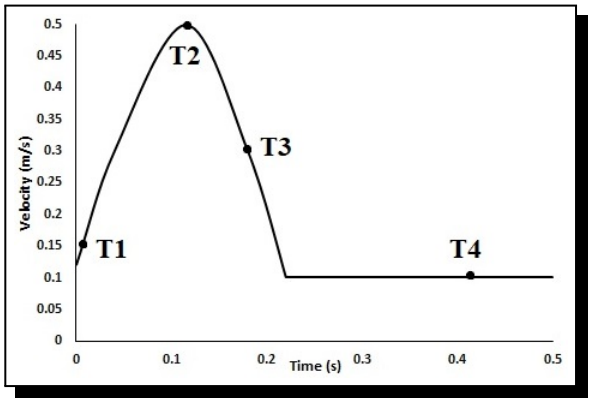

Figure 2. Time-dependent inlet velocity with T1 = 0.0015s, T2 = 0.1125s, T3 = 0.1875s, T4 = 0.4125s

3.1 Pressure and Velocity Distribution

The pressure distribution varies slightly along Model A due to the curvature and bifurcation. In Model B the effect of stenosis is seen to highly effect the pressure distribution, maximum pressure drop is recorded at T2 (Figure 3).

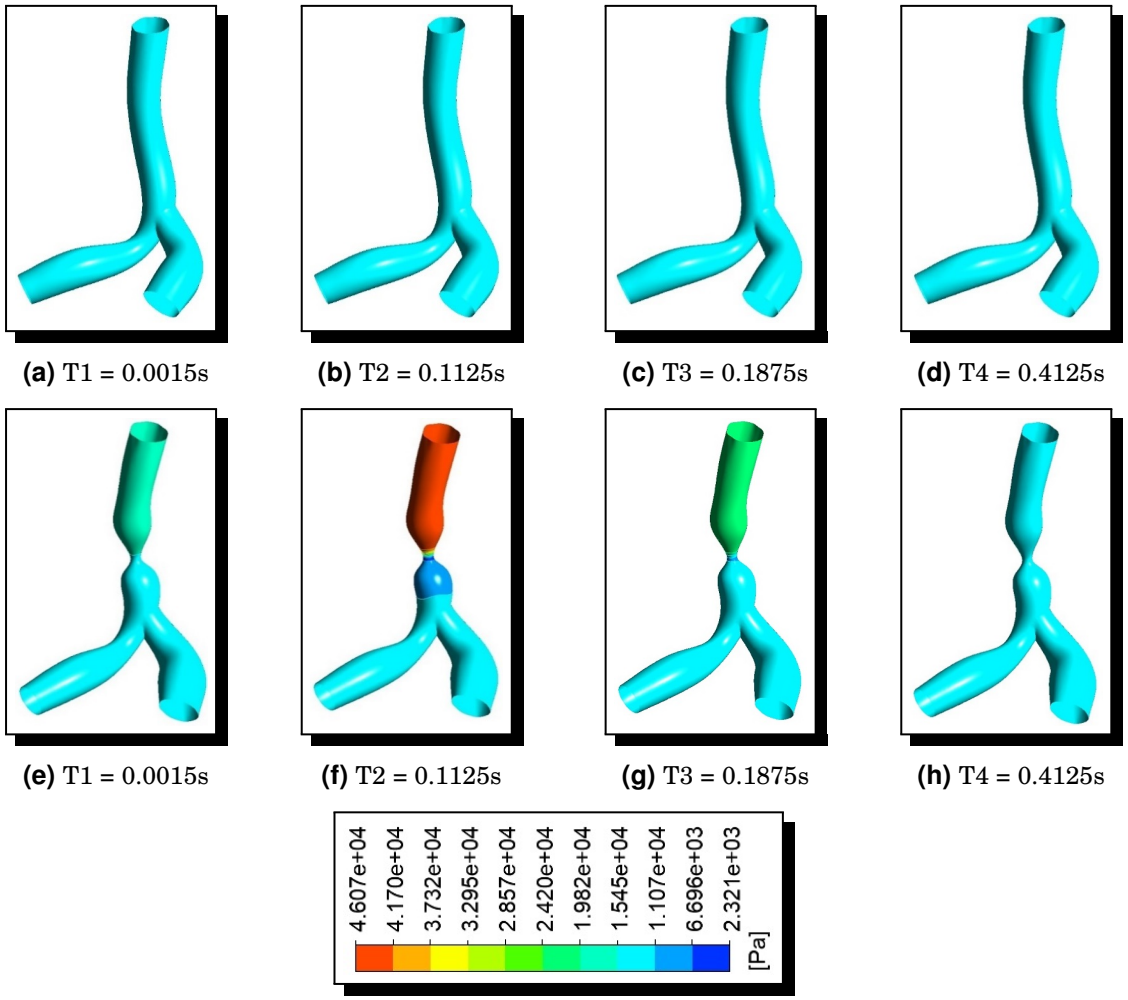

Figure 3. Pressure contours in Model A (a), (b), (c), (d) and in Model B (e), (f), (g), (h) at time instances T1, T2, T3 and T4

The 3D velocity streamlines in Figure 4 illustrate the changes in flow features with time and due to the stenosis. In Model A, at the beginning of the cardiac cycle at time T1 the flow appears to be laminar (Figure 4a). As we proceed along the cardiac cycle at peak systole (Figure 4b), the velocity magnitude increases throughout the geometry with maximum velocity in the infrarenal aorta region due to the curvature; as the flow bifurcates into the left and right common iliac arteries, swirling of flow is evident in the right iliac. The angle of bifurcation, positioning from the aorta and the curvature of the iliac arteries affects the division of flow. At T3 (Figure 4c) in the deceleration phase, recirculation is observed in the left iliac as well. At T4 the flow disturbances are spread out and swirling flow can still be seen in the right iliac (Figure 4d).

In Model B the flow of blood is studied considering the influence of severe stenosis. At T1 (Figure 4e), the velocity magnitude increases in the stenotic region due to a sudden decrease in cross-sectional area and in the post stenotic region due to a sudden increase in the cross-sectional area flow separation and recirculation is observed.

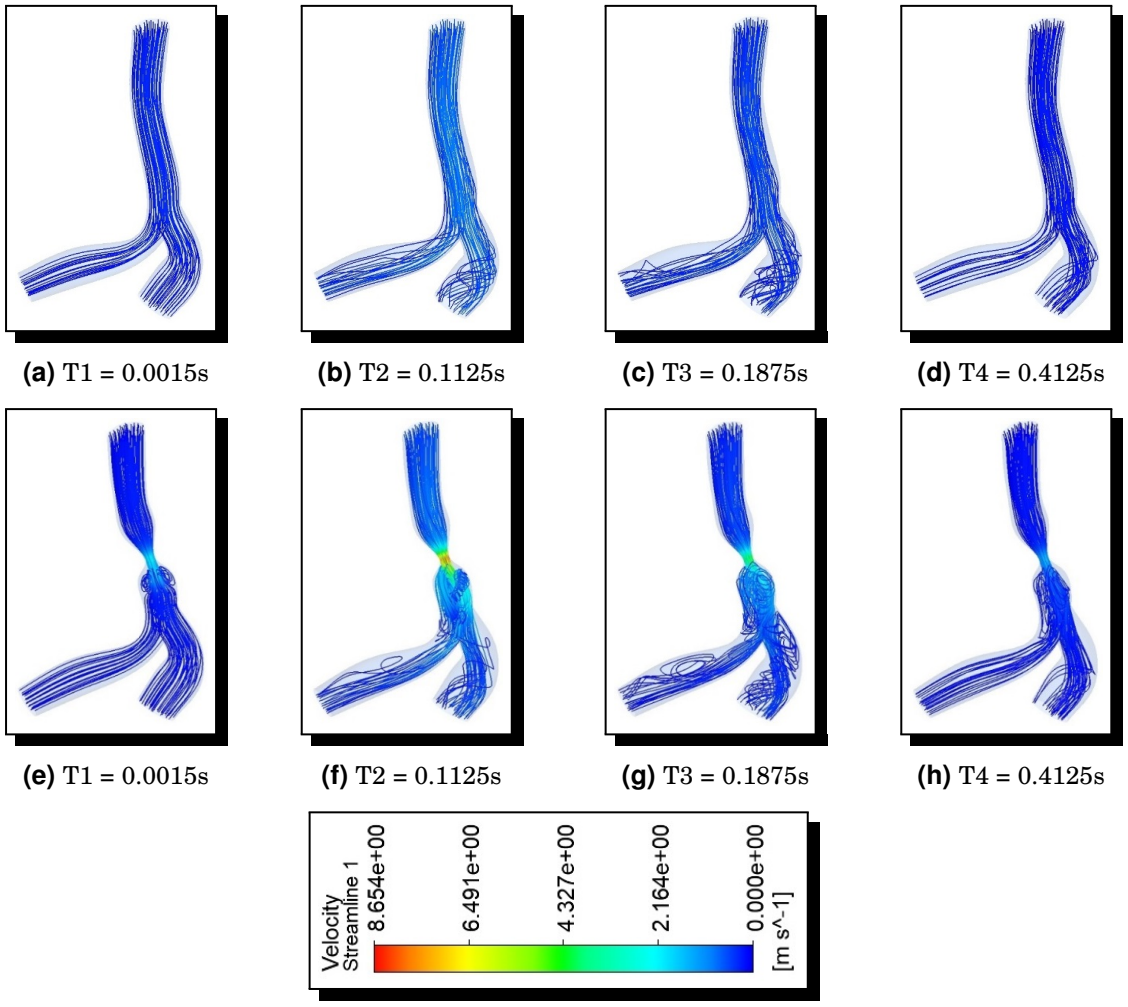

Figure 4. The velocity streamlines in Model A (a), (b), (c), (d) and in Model B (e), (f), (g), (h) at time instances T1, T2, T3 and T4

At T2 (Figure 4f), peak velocity is obtained with maximum velocity magnitude at the throat of stenosis. In the post stenotic region, there is an increase in flow separation with a magnification of the recirculation zone and an increase in swirling flow in the iliac arteries. At T3, in the deceleration phase the flow becomes chaotic with amplification of the recirculation vortex and development of new recirculation zones in the iliac arteries is observed (Figure 4g). As the flow reaches its minimum velocity at T4 (Figure 4h), the recirculation zone in the left iliac fades out, the recirculation and separation in the close proximity of the stenosis can still be observed with a decrease in swirling in the right iliac. The maximum velocity range increases nearly 8 times due to severe stenosis.

The velocity profile in Figures 5a–5d shows that the flow is laminar throughout the cardiac cycle but the amplitude of velocity profile varies for both models. The velocity profile near the wall is not plotted for Model B as the flow of blood gets affected due to the stenosis and deviates from the wall. This affects the proper supply of blood to the artery wall and in turn reduces the optimal supply of oxygen and other nutrients.

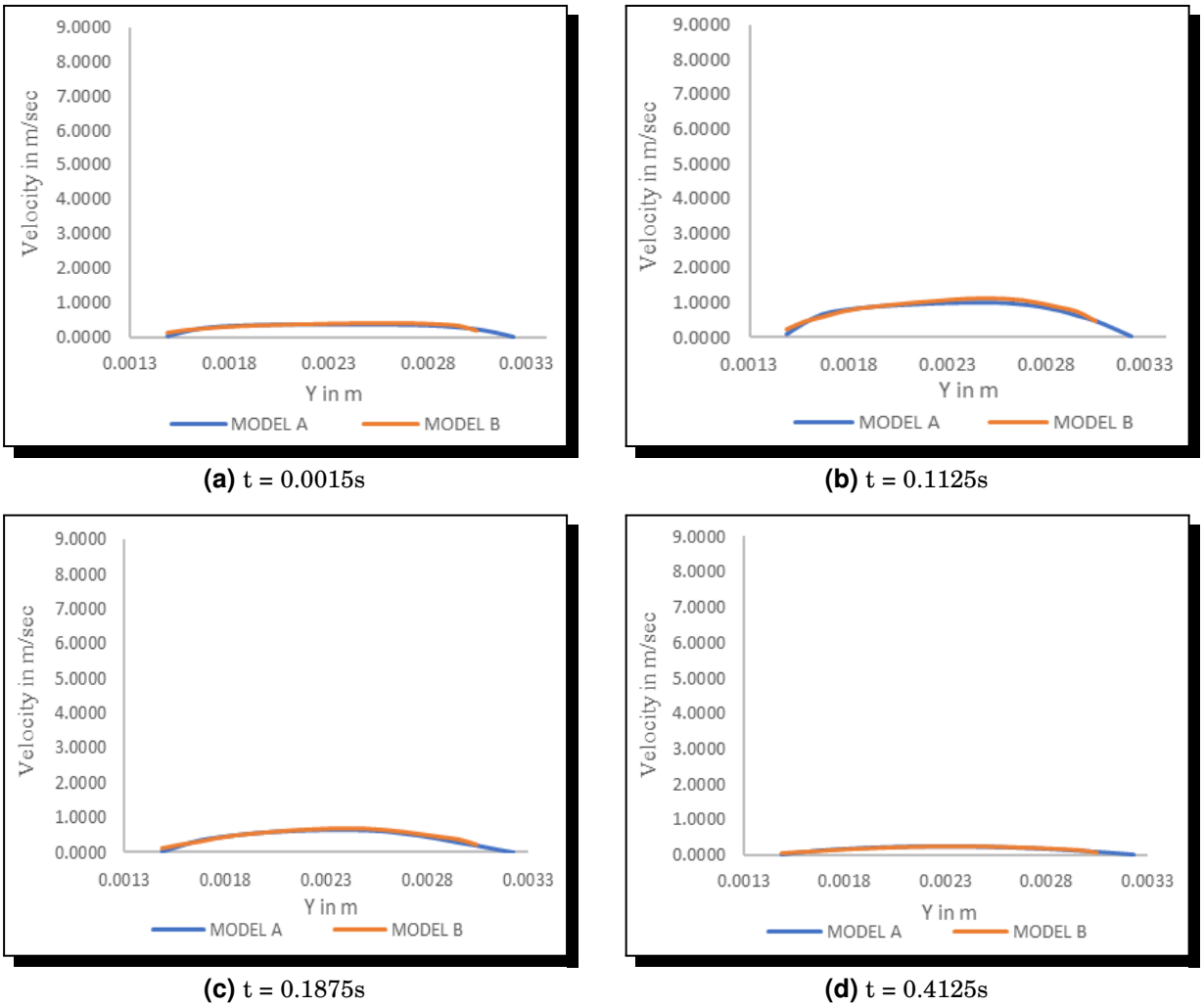

(a) t = 0.0015s **(b)** t = 0.1125s

(c) t = 0.1875s **(d)** t = 0.4125s

Figure 5. Velocity profile at P1

The velocity profile at the throat of the stenosis in Figures 6a–6d is laminar in Model A while in model B it appears to be turbulent. Owing its asymmetry to the formation of vortices and curvature of the artery [23, 33]. The amplitude of the velocity profile along with the maximum velocity ($v_{\max}$) in Model A and B varies throughout the cardiac cycle. At T1 in Model A and Model B $v_{\max}$ is recorded as 0.364 m/s and 3.500 m/s, respectively, this difference is because of the decrease in cross-sectional area which increases the resistance offered to the blood flow. At T2, the velocity acquires its peak with $v_{\max}$ increasing to 1.075 m/s and 8.655 m/s in Model A and B, respectively. The velocity profile also exhibits maximum asymmetry at T2. At T3, $v_{\max}$ reduces to 0.739 m/s and 4.944 m/s in Model A and B, respectively. Further decrease in maximum velocity is observed at T4 as for Model A and Model B, $v_{\max}$ = 0.247 m/s and 1.957 m/s, respectively.

The velocity profiles in Figure 7a–7d depict that the flow in Model A remains laminar. As blood flows through the stenosis with high velocity into the post stenotic region, it results in flow separation into the jet flow and recirculation zones. The shape of the velocity profiles for Model B also suggests the occurrence and interaction of the jet and recirculation zone. The higher peak in the velocity profile is of the jet. At time instances T1, T2, T3 and T4 there is

a change in amplitude of the velocity profile with time. The lower peak represents the velocity of the recirculation which varies throughout the cardiac cycle and is the maximum at T2.

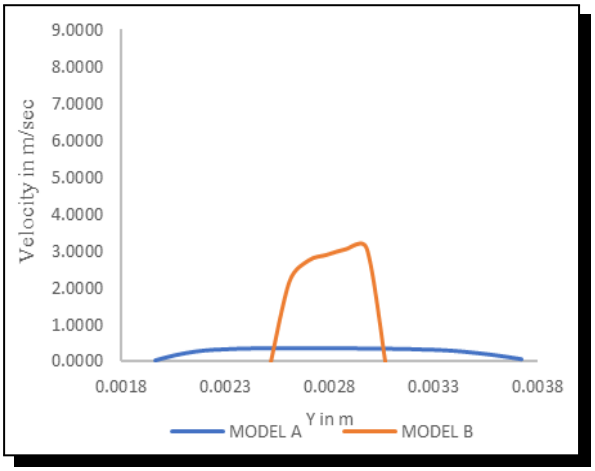

(a) t = 0.0015s

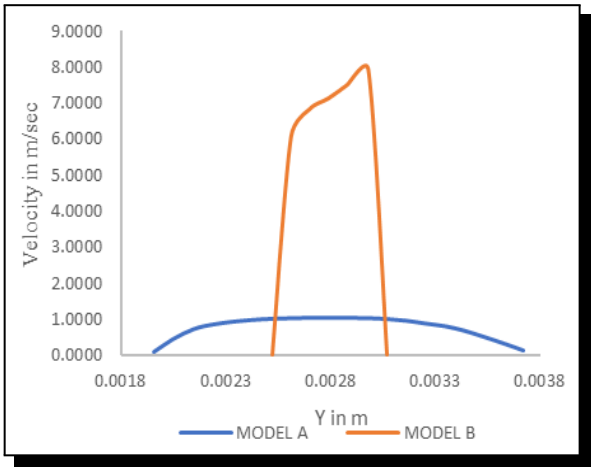

(b) t = 0.1125s

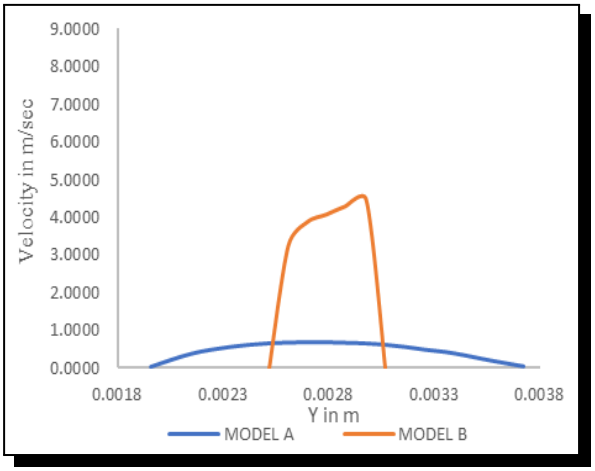

(c) t = 0.1875s

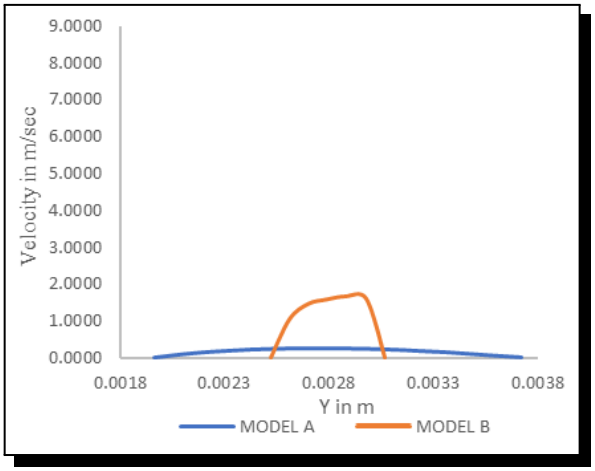

(d) t = 0.4125s

Figure 6. Velocity profile at P2

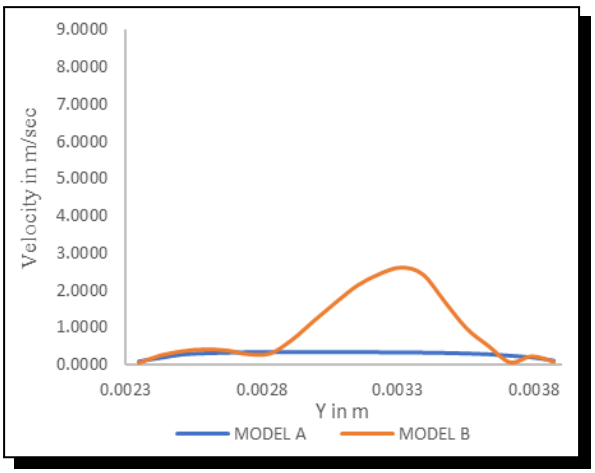

(a) t = 0.0015s

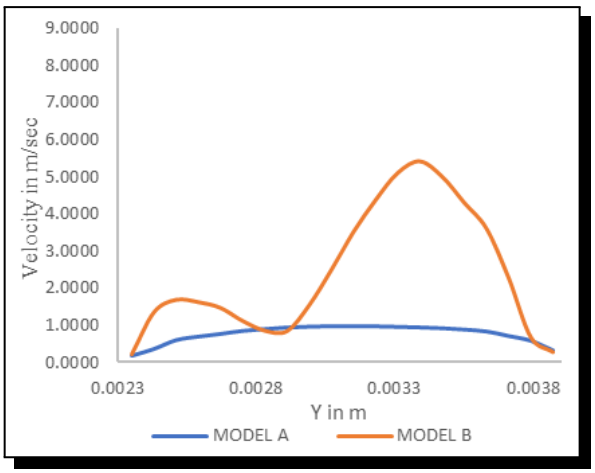

(b) t = 0.1125s

Figure Contd.

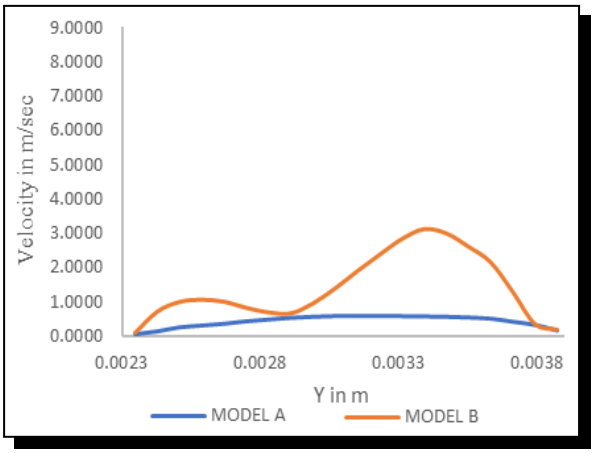

(c) t = 0.1875s

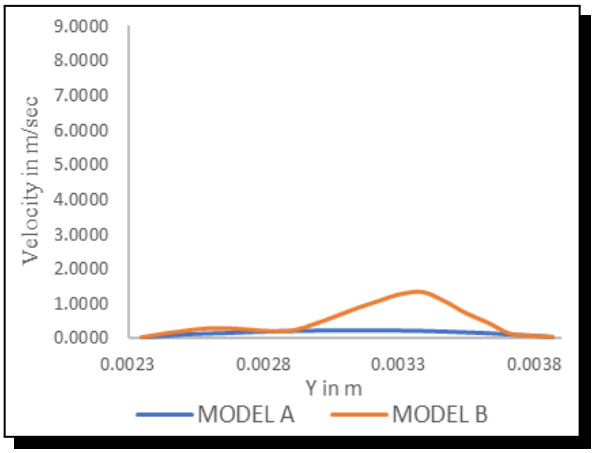

(d) t = 0.4125

Figure 7. Velocity profile at P3

3.2 Wall Shear Stress (WSS) and Oscillating Shear Index (OSI) Distribution

Wall Shear stress modulates the functions of endothelial cells which form the lining of the human vasculature and in turn triggers the process of atherosclerosis (Cheng *et al*. [13], and Okamoto *et al*. [27]). The wall shear stress distribution in Model A and Model B was studied throughout the cardiac cycle. In Model A the WSS variation is maximum at peak velocity (Figure 8b). In Model B the WSS variation is seen majorly at the throat of stenosis.

Figure 8e–8h. The maximum WSS is observed at T2 at the throat of the stenosis which makes the atherosclerotic plaque susceptible to rupture. Low and oscillating WSS plays a major role in the initiation of atherosclerosis. Hence, WSS based indicator, Oscillating shear Index (OSI) is calculated and its distribution along the wall is shown in Figure 9.

OSI is an important metric of WSS which measures the deflection of WSS from its established direction. In Model A, at T1 maximum OSI is recorded at the origin of the right iliac Figure 8a, OSI greater than 0.15 is considered high (Lee *et al*. [20]). At T2 there is an increase in regions of high OSI, a large area of high OSI is reflected at the curvature in the infrarenal aorta and small regions of high OSI are seen in both the iliac arteries (Figure 9b). At T3 (Figure 9c) no major changes are seen in the OSI pattern. A decrease in the oscillatory nature of WSS is noticed at T4 (Figure 9d). In Model B we see that severe stenosis results in an increase of change in direction of WSS which in turn can disrupt the alignment of endothelial cells and an increase in proliferation of LDL will aid in the progression of the disease and development of secondary stenosis.

3.3 Turbulent Kinetic Energy

Turbulence can be quantitatively analysed by turbulent kinetic energy (TKE), the process involving the production and dissipation of which has been termed as *kinetic energy cascade* (Pope [32]). The turbulent kinetic energy and turbulence dissipation rate have been modelled through the transport equations in the two-equation k-ε model. The variation of turbulent kinetic energy throughout the cardiac cycle was studied for Model B and plotted in Figure 10a–10d. A cardioid shaped region with higher values of TKE is identified at T2 in Figure 10b, with

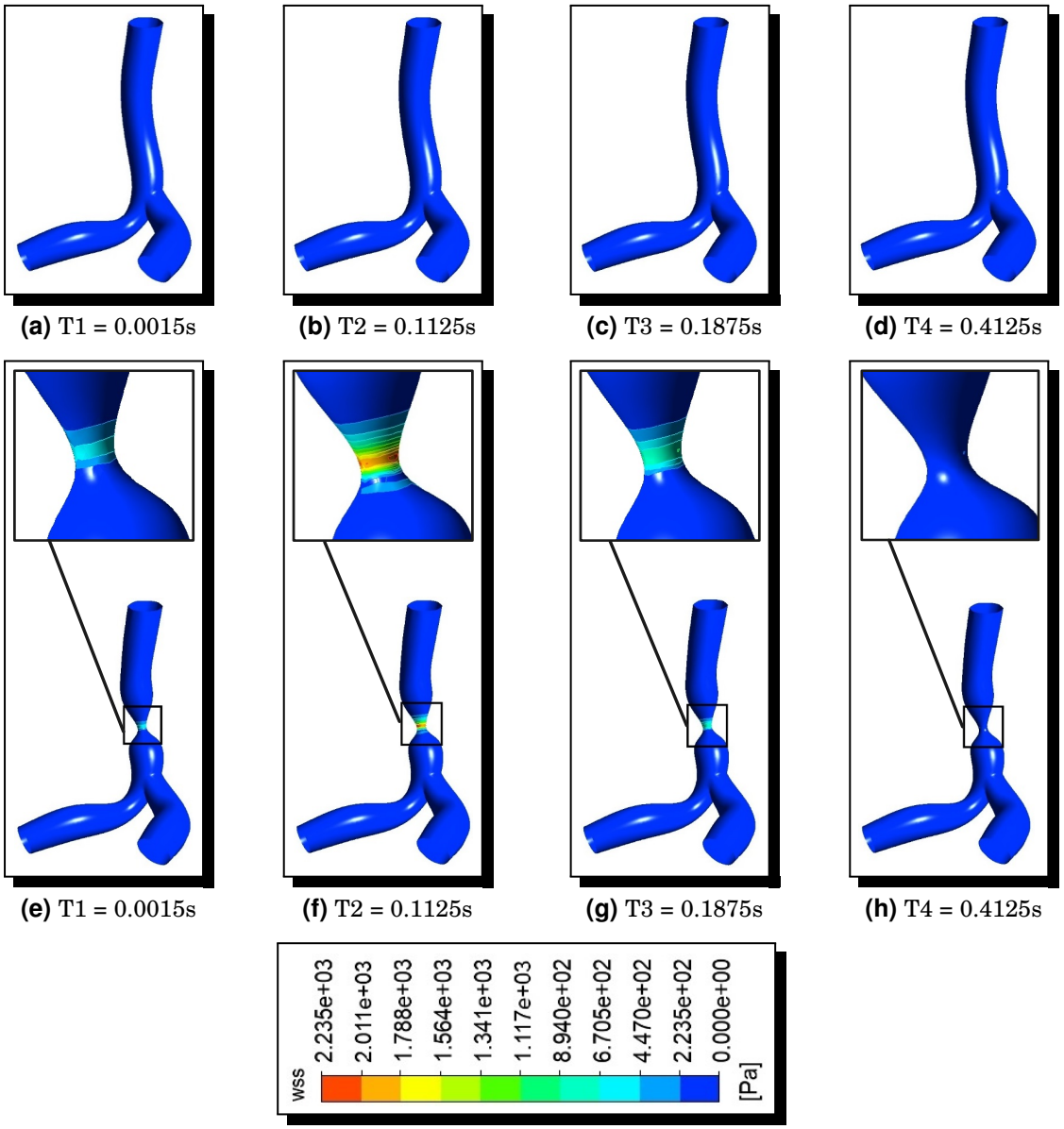

Figure 8. The WSS in Model A at time instances (a), (b), (c), (d) and in Model B at time instances (e), (f),(g), (h)

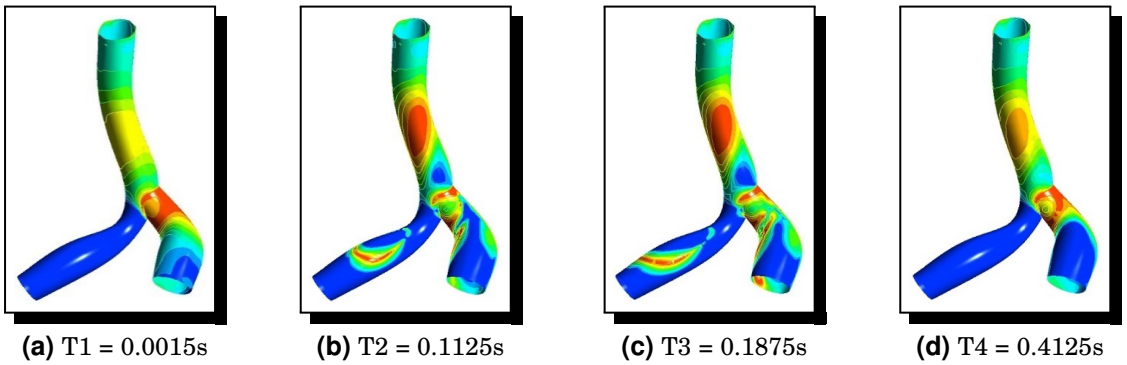

Figure Contd.

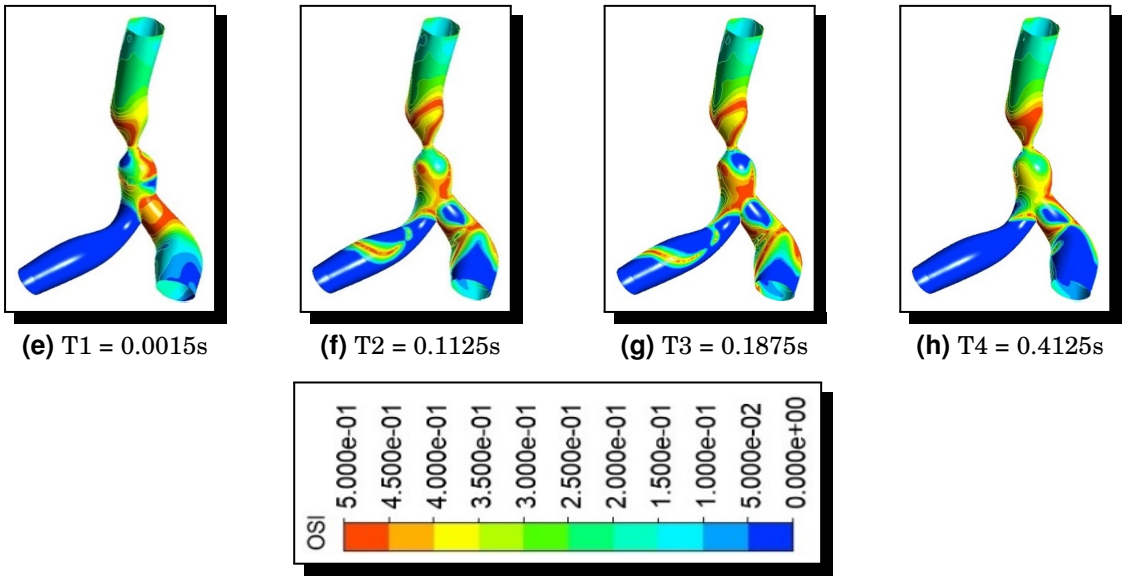

Figure 9. The OSI distribution in Model A at time instances (a), (b), (c), (d) and in Model B at time instances (e), (f), (g), (h)

maximum TKE, $\text{TKE}_{\text{max}} = 6.520\,\text{m}^2\text{s}^{-2}$ in the post stenotic region. In the deceleration phase the region of higher TKE reduces in area and the highest TKE recorded at T3 is $2.608\,\text{m}^2\text{s}^{-2}$. Further decrease in TKE is seen at T4, with TKE ranging between 4.551e-13 m^2s^{-2} to 6.520e-01 m^2s^{-2}.

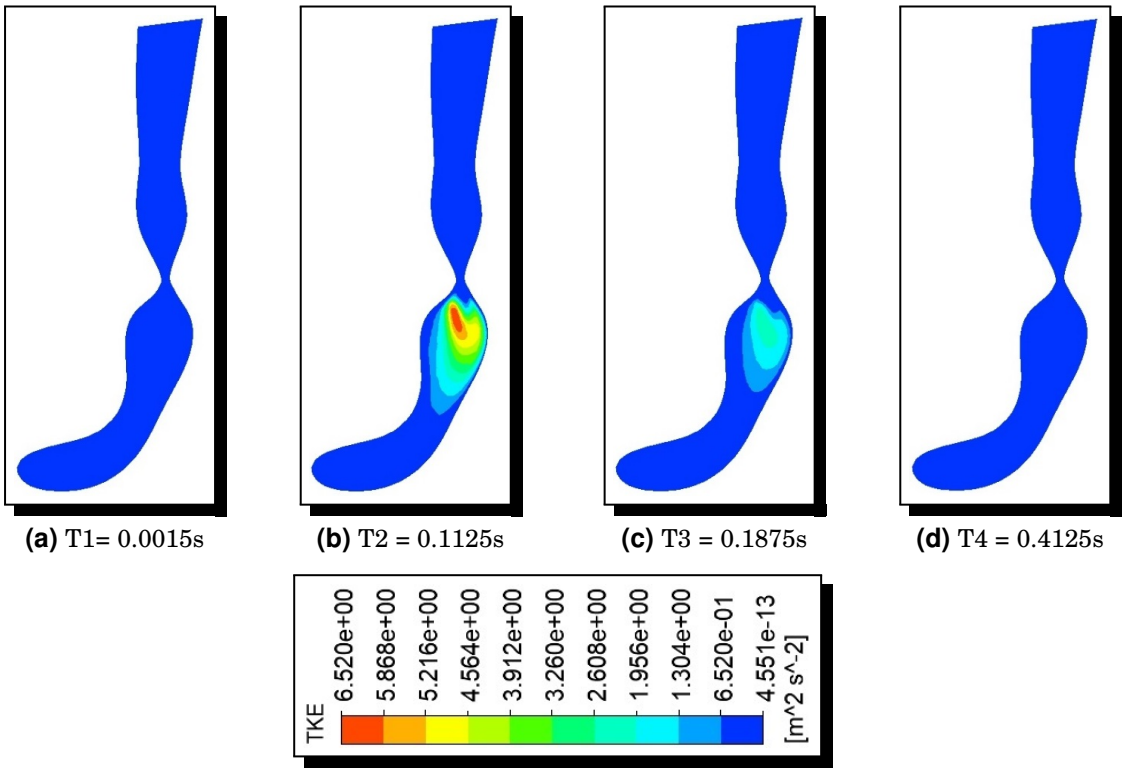

Figure 10. The TKE on transverse plane in Model B (a), (b), (c), (d) at time instances T1, T2, T3 and T4

4. Conclusion

The study of hemodynamic and biochemical processes involved in the inception and development of arterial diseases have proved to be instrumental in development of latest clinical intervention techniques. The pulsatile nature of blood makes it important to examine the flow behavior; changes in hemodynamic parameters are eminent throughout the cardiac cycle in aortoiliac bifurcation with aortic stiffness. Significant changes in the values of the hemodynamic parameters were observed at the peak systole. The hemodynamic parameters were assessed locally in the pre stenotic region, throat of the stenosis and in the post stenotic region. The laminar flow transitions into turbulent flow together with the emergence of jet flow, recirculation and separation zones. The turbulent energy was maximum in case of severe stenosis at peak systole. The turbulence in blood flow effects the arrangement of endothelial cells of the lumen, the study of which may prove to be an important factor of disease prognosis. The Aortoiliac occlusive disease has yet not been fully explored; hence, the present numerical study assists in deciphering the interplay of pulsatile blood flow, hemodynamic parameters, blood flow patterns and arterial geometry in AIOD.

Competing Interests

The authors declare that they have no competing interests.

Authors' Contributions

All the authors contributed significantly in writing this article. The authors read and approved the final manuscript.

References

[1] M. Abbasian, M. Shams, Z. Valizadeh, A. Moshfegh, A. Javadzadegan and S. Cheng, Velocity measurements in steady flow through axisymmetric stenoses at moderate Reynolds numbers, *Computer Methods and Programs in Biomedicine* **186** (2020), 105185, DOI: 10.1016/j.cmpb.2019.105185.

[2] S. A. Ahmed and D. P. Giddens, Velocity measurements in steady flow through axisymmetric stenoses at moderate Reynolds numbers, *Journal of Biomechanics* **16**(7) (1983), 505 – 516, DOI: 10.1016/0021-9290(83)90065-9.

[3] S. A. Ahmed and D. P. Giddens, Flow disturbance measurements through a constricted tube at moderate Reynolds numbers, *Journal of Biomechanics* **16**(12) (1983), 955 – 963, DOI: 10.1016/0021-9290(83)90096-9.

[4] M. H. Amiri, A. Keshavarzi, A. Karimipour, M. Bahiraei, M. Goodarzi and J. Esfahani, A 3-D numerical simulation of non-Newtonian blood flow through femoral artery bifurcation with a moderate arteriosclerosis: investigating Newtonian/non-Newtonian flow and its effects on elastic vessel walls, *Heat and Mass Transfer* **55**(7) (2019), 2037 – 2047, DOI: 10.1007/s00231-019-02583-4.

[5] J. Wendt, *Computational Fluid Dynamics: An Introduction*, Springer, Berlin—Heidelberg, 291 pages (2013).

[6] M. Andayesh, A. Shahidian and M. Ghassemi, Numerical investigation of renal artery hemodynamics based on the physiological response to renal artery stenosis, *Biocybernetics and Biomedical Engineering* **40**(4) (2020) 1458 – 1468, DOI: 10.1016/j.bbe.2020.08.006.

[7] A. Banerjee, S. Chen, L. Pasea, A. G. Lai, M. Katsoulis, S. Denaxas, V. Nafilyan, B. Williams, W. K. Wong, A. Bakhai, K. Khunti, D. Pillay, M. Noursadeghi, H. Wu, N. Pareek, D. Bromage, T. A. McDonagh, J. Byrne, J. T. H. Teo, A. M. Shah, B. Humberstone, L. V. Tang, A. S. V. Shah, A. Rubboli, Y. Guo, Y. Hu, C. L. M. Sudlow, G. Y. H. Lip and H. Hemingway, Excess deaths in people with cardiovascular diseases during the COVID-19 pandemic, *European Journal of Preventive Cardiology* **28**(14) (2021), 1599 – 1609, DOI: 10.1093/eurjpc/zwaa155.

[8] T. Barber, Wall shear stress and near-wall flows in the stenosed femoral artery, *Computer Methods in Biomechanics and Biomedical Engineering* **20**(10) (2017), 1048 – 1055, DOI: 10.1080/10255842.2017.1331342.

[9] A. Bit, A. Alblawi, H. Chattopadhyay, Q. A. Quais, A. C. Benim, M. Rahimi-Gorji and H. T. Do, Three dimensional numerical analysis of hemodynamic of stenosed artery considering realistic outlet boundary conditions, *Computer Methods and Programs in Biomedicine* **185** (2020), 105163, DOI: 10.1016/j.cmpb.2019.105163.

[10] F. Carneiro, V. G. Ribeiro, J. Teixeira and S. Teixeira, Numerical study of blood fluid rheology in the abdominal aorta, *WIT Transactions on Ecology and the Environment* **114** (2008), 169 – 178, DOI: 10.2495/DN080181.

[11] V. Carvalho, F. Carneiro, A. C. Ferreira, V. Gama, J. C. Teixeira and S. Teixeira, Numerical study of the unsteady flow in simplified and realistic iliac bifurcation models, *Fluids* **6**(8) (2021), 284, DOI: 10.3390/fluids6080284.

[12] V. Carvalho, D. Pinho, R. A. Lima, J. C. Teixeira and S. Teixeira, Blood flow modeling in coronary arteries: A review, *Fluids* **6**(2) (2021), 53, DOI: 10.3390/fluids6020053.

[13] H. Cheng, W. Zhong, L. Wang, Q. Zhang, X. Ma, Y. Wang, S. Wang, C. He, Q. Wei and C. Fu, Effects of shear stress on vascular endothelial functions in atherosclerosis and potential therapeutic approaches, *Biomedicine & Pharmacotherapy* **158** (2023), 114198, DOI: 10.1016/j.biopha.2022.114198.

[14] C. Clark, Turbulent velocity measurements in a model of aortic stenosis, *Journal of Biomechanics* **9**(11) (1976), 677 – 687, DOI: 10.1016/0021-9290(76)90169-X.

[15] S. Engelhard, M. van Helvert, J. Voorneveld, J. G. Bosch, G. P. R. Lajoinie, M. Versluis, E. G. Jebbink and M. M. P. J. Reijnen, US velocimetry in participants with aortoiliac occlusive disease, *Radiology* **301**(2) (2021), 332 – 338, DOI: 10.1148/radiol.2021210454.

[16] S. Engelhard, M. van Helvert, J. Voorneveld, J. G. Bosch, G. Lajoinie, E. G. Jebbink, M. M. P. J. Relijnen and M. Versluis, blood flow quantification with high-frame-rate, contrast-enhanced ultrasound velocimetry in stented aortoiliac arteries: In vivo feasibility, *Ultrasound in Medicine and Biology* **48**(8) (2022), 1518 – 1527, DOI: 10.1016/j.ultrasmedbio.2022.03.016.

[17] M. A. Faghy, J. Yates, A. P. Hills, S. Jayasinghe, C. da Luz Goulart, R. Arena, D. Laddu, R. Gururaj, S. K. Veluswamy, S. Dixit and R. E. Ashton, Cardiovascular disease prevention and management in the COVID-19 era and beyond: An international perspective, *Progress in Cardiovascular Diseases* **76** (2023), 102 – 111, DOI: 10.1016/j.pcad.2023.01.004.

[18] M. Gay and L. T. Zhang, Numerical studies of blood flow in healthy, stenosed, and stented carotid arteries, *International Journal for Numerical Methods in Fluids* **61**(4) (2009), 453 – 472, DOI: 10.1002/fld.1966.

[19] E. G. Karvelas, N. K. Lampropoulos, T. E. Karakasidis and I. E. Sarris, Blood flow and diameter effect in the navigation process of magnetic nanocarriers inside the carotid artery, *Computer Methods and Programs in Biomedicine* **221** (2022), 106916, DOI: 10.1016/j.cmpb.2022.106916.

[20] S. W. Lee, L. Antiga and D. A. Steinman, Correlations among indicators of disturbed flow at the normal carotid bifurcation, *Journal of Biomechanical Engineering* **131**(6) (2009), 061013, DOI: 10.1115/1.3127252.

[21] P. Libby, J. E. Buring, L. Badimon, G. K. Hansson, J. Deanfield, M. S. Bittencourt, L. Tokgözoğlu and E. F. Lewis, Atherosclerosis, *Nature Reviews Disease Primers* **5** (2019), Article number: 56, DOI: 10.1038/s41572-019-0106-z.

[22] D. Lopes, H. Puga, J. Teixeira and R. Lima, Blood flow simulations in patient-specific geometries of the carotid artery: A systematic review, *Journal of Biomechanics* **111** (2020), 110019, DOI: 10.1016/j.jbiomech.2020.110019.

[23] Z. Malota, J. Glowacki, W. Sadowski and M. Kostur, Numerical analysis of the impact of flow rate, heart rate, vessel geometry, and degree of stenosis on coronary hemodynamic indices, *BMC Cardiovascular Disorders* **18**(1) (2018), Article number: 132, DOI: 10.1186/s12872-018-0865-6.

[24] U. Morbiducci, A. M. Kok, B. R. Kwak, P. H. Stone, D. A. Steinman and J. J. Wentzel, Atherosclerosis at arterial bifurcations: evidence for the role of haemodynamics and geometry, *Thrombosis and Haemostasis* **115**(03) (2016), 484 – 492, DOI: 10.1160/TH15-07-0597.

[25] J. Moradicheghamahi, J. Sadeghiseraji and M. Jahangiri, Numerical solution of the Pulsatile, non-Newtonian and turbulent blood flow in a patient specific elastic carotid artery, *International Journal of Mechanical Sciences* **150** (2019) 393 – 403, DOI: 10.1016/j.ijmecsci.2018.10.046.

[26] S. Nadeem, S. Ali, N. Akkurt, M. B. B. Hamida, S. Almutairi, H. A. Ghazwani, S. M. Eldin, Z. A. Khan and A. Al-Shafay, Modeling and numerical simulation of non-Newtonian arterial blood flow for mild to severe stenosis, *Alexandria Engineering Journal* **72** (2023), 195 – 211, DOI: 10.1016/j.aej.2023.03.088.

[27] T. Okamoto, E. J. Park, E. Kawamoto, H. Usuda, K. Wada, A. Taguchi and M. Shimaoka, Endothelial connexin-integrin crosstalk in vascular inflammation, *Biochimica et Biophysica Acta (BBA) - Molecular Basis of Disease* **1867**(9) (2021), 166168, DOI: 10.1016/j.bbadis.2021.166168.

[28] C. Oliveira, A. A. Soares, A. Simões, S. Gonzaga and A. Rouboa, Numerical study of non-Newtonian blood behavior in the abdominal aortic bifurcation of a patient-specific at rest, *The Open Sports Sciences Journal* **10**(1) (2017), 279 – 285, DOI: 10.2174/1875399X01710010279.

[29] M. J. Paisley, S. Adkar, B. M. Sheehan and J. R. Stern, Aortoiliac occlusive disease, *Seminars in Vascular Surgery* **35**(2) (2022), 162 – 171, DOI: 10.1053/j.semvascsurg.2022.04.005.

[30] R. Pandey, M. Kumar, J. Majdoubi, M. Rahimi-Gorji and V. K. Srivastav, A review study on blood in human coronary artery: Numerical approach, *Computer Methods and Programs in Biomedicine* **187** (2020), 105243, DOI: 10.1016/j.cmpb.2019.105243.

[31] R. Pandey, M. Kumar and V. K. Srivastav, Numerical computation of blood hemodynamic through constricted human left coronary artery: Pulsatile simulations, *Computer Methods and Programs in Biomedicine* **197** (2020), 105661, DOI: 10.1016/j.cmpb.2020.105661.

[32] S. B. Pope, *Turbulent Flows*, Cambridge University Press, Cambridge (2012), DOI: 10.1017/CBO9780511840531.

[33] A. Rashid, S. A. Iqrar, A. Rashid and M. Simka, Results of numerical modeling of blood flow in the internal jugular vein exhibiting different types of strictures, *Diagnostics* **12**(1) (2022), 2862, DOI: 10.3390/diagnostics12112862.

[34] M. L. Rizzini, A. Candreva, C. Chiastra, E. Gallinoro, K. Calò, F. D'Ascenzo, B. De Bruyne, T. Mizukami, C. Collet, D. Gallo and U. Morbiducci, Modelling coronary flows: Impact of differently measured inflow boundary conditions on vessel-specific computational hemodynamic profiles, *Computer Methods and Programs in Biomedicine* **221** (2022), 106882, DOI: 10.1016/j.cmpb.2022.106882.

[35] V. Z. Rocha, F. H. Rached and M. H. Miname, Insights into the role of inflammation in the management of atherosclerosis, *Journal of Inflammation Research* **16** (2023), 2223 – 2239, DOI: 10.2147/JIR.S276982.

[36] M. Sinnott, P. W. Cleary and M. Prakash, An investigation of pulsatile blood flow in a bifurcation artery using a grid-free method, in: *Proceedings of the Fifth International Conference on CFD in the Process Industries* (CSIRO, Melbourne, Australia, 13-15 December 2006), pp. 1 – 5 (2006).

[37] B. Thomas, K. S. Sumam and N. Sajikumar, Patient specific modelling of blood flow in coronary artery, *Journal of Applied Fluid Mechanics* **14**(5) (2021), 1469 – 1482, DOI: 10.47176/JAFM.14.05.32186.

[38] M. Vaduganathan, G. A. Mensah, J. V. Turco, V. Fuster and G. A. Roth, The global burden of cardiovascular diseases and risk: A compass for future health, *Journal of the American College of Cardiology* **80**(25) (2022), 2361 – 2371, DOI: 10.1016/j.jacc.2022.11.005.

[39] N. M. Wilson, A. K. Ortiz and A. B. Johnson, The vascular model repository: A public resource of medical imaging data and blood flow simulation results, *Journal of Medical Devices* **7**(4) (2013), 040923, DOI: 10.1115/1.4025983.

[40] D. F. Young, Effect of a time-dependent stenosis on flow through a tube, *Journal of Engineering for Industry* **90**(2) (1968), 248 – 254, DOI: 10.1115/1.3604621.